Effect of Different Surface Profile on Wear of Rail Steel (AS1085.1) used in Australian heavy-haul railways

Asitha C. Athukorala
Queensland University of Technology
Brisbane, QLD 4000, Australia
asitha.athukoralalage@qut.edu.au

I. U. Wickramasinghe
Queensland University of Technology
Brisbane, QLD 4000, Australia

Dennis V. De Pellegrin
Queensland University of Technology
Brisbane, QLD 4000, Australia

Asitha Athukorala* is PhD student at the Queensland University of Technology, Brisbane, Australia. His research area include wear regime of rail wheel contact interface, material ratcheting behaviour of rail steel, surface roughness evolution of contact interface and their effects on the wear mechanism.

Isuru Wickramashinghe completes his PhD in the Queensland University of Technology, Brisbane, Australia. His thesis based on the rail surface wear mechanism at different wear profile and modelling wear of rail steel using ratcheting behaviour of rail steel.

Dennis De Pellegrin completed his PhD with distinction in the field of tribology in 2003 at the University of Western Australia. In 2004 he moved to Trinity College Dublin (Ireland) after being awarded an Irish Research Council postdoctoral fellowship. He has now joined Queensland University of Technology as a senior lecturer, where he is engaged in teaching, supervision of QUT's Formula SAE team and research in many areas related to tribology.

Abstract— The extreme diversity of conditions acting on railways necessitates a variety of experimental approaches to study the critical wear mechanisms that present themselves at the contact interface. This work investigates the effects of contact pressure and geometry in rolling-contact wear tests by using discs with different radii of curvature to simulate the varying contact conditions that may be typically found in the field. It is commonly adapted to line contact interface as it has constant contact pressure. But practical scenario of the rail wheel interface, the contact area increase and contact pressure change as tracks worn off.

The tests were conducted without any significant amount of traction, but micro slip was still observed due to contact deformation. Moreover, variation of contact pressure was observed due to contact patch elongation and diameter reduction. Rolling contact fatigue, adhesive and sliding wear were observed on the curved contact interface. The development of different wear regimes and material removal phenomena were analysed using microscopic images in order to broaden the understanding of the wear mechanisms occurring in the rail-wheel contact.

Keywords— rolling-contact, twin-disc, hardened rail, wear rate

1. Introduction

The aspects of wear, friction and fatigue are very important in the operation of railways. Significant research exists that deals with identifying the wear and fatigue mechanisms within the rail-wheel contact. Despite significant progress, it remains very difficult to model all aspects of the contact due to deviations in material composition, inhomogeneous material properties, distinct contact behaviour, environmental effects and numerous other uncontrolled variables. Therefore, different approaches are necessary to identify different phases of wear and fatigue behaviour in the rail-wheel contact, eventually making it possible to minimize the problems of unexpected wear and fatigue failure.

Wear occurs by mechanical and/or chemical means and is accelerated by frictional heating. Wear is defined as the removal of solid material from the rubbing surfaces (Bhushan, 2013) and can be found mainly in three forms: adhesive, abrasive and rolling contact fatigue (RCF) wear. In the field of rail-wheel contact, RCF wear can be observed more frequently (R. Lewis & Dwyer-Joyce, 2004). The rail material is repeatedly loaded as the train passes over the rail. The train's weight is transmitted from the wheels to the rail surface through tiny contact areas that experience large contact stresses (R. Lewis & Olofsson, 2009). When the maximum contact pressure exceeds the elastic limit (yield strength) of the rail material, this leads to plastic deformation called ratcheting. Accumulated plastic strain may eventually lead to material detachment from the parent material's surface in the form of wear particles. Trapped particles within the contact interfaces can accelerate wear as well as change the wear mechanism. The particle itself can provide evidence for a particular wear mechanism like adhesion, abrasion, RCF or a mixture of these.

The different wear mechanisms acting on rail wheel contact interface have been studied experimentally, with the use of twin disc rail simulators, by various researchers (Green, Rainforth et al., 2007). In particular, focus has been set on the contributing factors like: slip (Pal, Daniel et al., 2012), pressure, lubrication (Ozsarac & Aslanlar, 2008) and microstructure. Further research is directed towards different types of damage on the rail head and their mechanism (Ringsberg, Loo-Morrey et al., 2000; Sheng & Kahraman, 2011; Vasic, Franklin et al., 2011). Moreover, extensive experimental research has been conducted on the different types of damage caused on the rail head and the associated mechanism contributing to this (e.g. Ringsberg, Loo-Morrey et al., 2000; Sheng & Kahraman, 2011; Vasic, Franklin et al., 2011). It has been identified that most of the damage mechanisms are driven by the ratcheting phenomenon taking place on the surface of the rail head. Several computational efforts have been made to explain the wear mechanisms and predict damage caused and accumulated by ratcheting mechanisms (e.g. Enblom & Berg, 2005; Franklin & Kapoor, 2007). However, there has been limited success in simulating accurately the RCF wear damage. This has been attributed primarily to the complexity of the ratcheting phenomenon but also due to the lack of appropriate material modelling. Modelling the inelastic behaviour of rail materials under complex cyclic loading conditions has been considered to be important for improving damage simulation. To this end, extensive experimental and computational research has been conducted on the identification of the ratcheting phenomenon characteristics and effective modelling and prediction (Chaboche, 2008; Dafalias, Kourousis et al., 2008; Feigenbaum, Dugdale et al., 2012; Kourousis & Dafalias, 2013; Krishna, Hassan et al., 2009).

The rail-head profile and rail curves make a substantial contribution to track degradation (Epp & Mutton, 2002; Evans, 2013). Rail profiles are distorted mainly due to wear and plastic deformation. The track surfaces are periodically ground to remove surface initiated cracks and deformed material layers in order to control profile distortion and the risk of rail fracture, but track surfaces are roughened to some extent by the grinding process. In addition, this process can cause the development of residual shear stress in the subsurface of the rail material that will ultimately affect the wear mechanism, particle generation and fatigue crack development. Broad understanding of the wear and contact fatigue behaviour is, therefore, essential.

Most of the relevant research has been conducted using twin disc rail simulator with flat-profile surfaces,

because the nominal contact pressure remains constant throughout the test. In contrast, this paper focuses on the effects of different contact pressures and profiles on wear and rolling contact fatigue mechanisms of Australian rail steel (AS1085.1) under dry (un-lubricated) conditions.

2. Experiment Setup

A. Twin Disc Test-Rig

The test-rig initially used by Marich and Mutton (Marich & Mutton, 1989) was significantly improved by Wilson et al. (Wilson, Hargreaves et al., 2006) for lubrication testing rather than rail material testing. The contact angle between the rolling discs is not variable, as is the case for some other test-rigs in the literature (Saulot, Descartes et al., 2009; Suda, Komine et al., 2002; Takikawa & Iriya, 2008).

The test-rig used for the experiments presented in this paper uses relatively large wheel and rail discs (300 and 150 mm in diameter approximately), is capable of high contact loads (up to 12kN) and of continuously running for large number of cycles (Jamison, 1982). The test-rig uses 5400 pulses per revolution incremental shaft encoders that are connected to the two shafts with belt drives to measure the rotational speed of the driving and driven discs. A calibrated load cell was used to measure the contact force from the pneumatic ram and all digital output signals were connected to a data acquisition system (DAQ system). The DAQ system uses the DAQ View interface to record the input signals. Pneumatic pressure was used to apply the contact load to the discs, and the rotational speed of the motor connected to the driving disc was controlled by a variable frequency motor controller.

B. Test Samples

Both rail and wheel disc samples were prepared according to the AS 1085.1-2002 material standard for rail and wheels ("Australian Standard : Railway Track Materials. Part 1: Steel Rails. AS1085.1-2002," 2002). The discs were casted at the QR National (Queensland Rail National) workshop and oil quenched to the standard hardness. These hardened samples were then machined to the test-rig dimensions. Comparison of the material composition of standard and sample materials is shown in Table I.

The small disc's outside surface curvature was machined differently for each disc (flat, 100mm, 50mm and 25mm diameter) to study the behaviour of the contact profile during wear and to apply different contact pressures.

C. Parameter Determination

1) Sliding Distance

In this experiment, no external torque was applied to the driven disc during the test procedure. Although operating under free-rolling conditions, micro slip was discerned, and fluctuated on average between 0.04 and 0.12 percent during the tests. The sliding distance over a given time interval $[t_0, t_1]$ may be given by,

$$\mathbf{S} = \int_{t_0}^{t_1} \boldsymbol{V_r} - \boldsymbol{V_w} dt \qquad (1)$$

Where V_r and V_w are the rail disc and wheel disc peripheral speeds respectively.

2) Contact Pressure

The maximum contact pressure P_o is calculated using the equation developed by Timoshenko and Goodier (Timoshenko & Goodier) for two elastically-identical cylindrical steel discs. As the load is applied a line contact forms between the test discs. The maximum contact pressure is given by,

$$\boldsymbol{P_o} = \mathbf{0.418}\sqrt{(\boldsymbol{PE})/\boldsymbol{R}} \qquad (2)$$

Where P is the load per unit length of the contact, and E is the effective Young's modulus and R is equivalent radius defined as,

$$\frac{1}{R} = \frac{1}{R_r} + \frac{1}{R_w} \quad (3)$$

Where R_w and R_r are the radii of wheel and rail test discs respectively.

3) Wear Rate

Wear is measured in terms of variation of the radii and the elongation of the contact patch during the test and wear volume can be subsequently calculated using the measured parameters. Wear rate may be analysed using Archard's wear law (Bolton & Clayton, 1984; Fries & Dávila, 1986; Hardwick, Lewis et al., 2014; Markov, 1995; Tyfour, Beynon et al., 1995) which defines the dimensionless wear coefficient (*K*) as the product of wear rate *k* (mm^3/N/mm) and hardness *H* (MPa) of the softer material in contact. But wear rate is not a material property, and it is defined as wear volume per unit distance, per unit load, i.e.,

$$k = \frac{V}{F_N S} \quad (4)$$

Where *V* is wear volume (mm^3), F_N is normal contact load (N), and *S* is the sliding distance (mm).

4) Million Gross Tonne (MGT)

The rail industry expresses rail traffic (fundamentally the loading condition of the rail) in terms of million gross tonne to simplify and combine the various loading conditions and number of loading cycles. So, one MGT is equivalent to moving one tonne of load, one million times across a given portion of rail surface. The following equation provides a mathematical representation of MGT,

$$MGT = \frac{F_N \times N}{g \times 1000 \times 1{,}000{,}000} \quad (5)$$

Where F_N is normal contact load (N) and *N* is number of cycles the load is applied.

3. Result and Discussion

A. Wear of Rail Discs

Prior to measurement of the diameter of the discs, the system was allowed to cool down to room temperature to reduce the effects of thermal expansion on any of the measurements. Measurements were recorded after the discs were cleaned properly using ethanol and hexane. Diameter reductions observed are presented in Figure 1.

As the discs have distinct curvatures at the contact line, diameter change does not give an accurate reflection of the wear behaviour of the rail-disc contact, as the worn area would vary due to the changing curvature of the discs. Therefore, the wear volumes were calculated using measurements of diameter and contact patch elongation. Table II provides clear statistics about the final condition of the rail discs. According to Table II, the contact patch elongated during the tests, and correspondingly the pressure has dropped. This kind of study on head-hardened rail steel is novel and isn't found in the literature. The calculated wear volume is plotted in Figure 2 against million gross tonnes (MGT), which is used in the rail industry to calculate annual rail traffic.

Comparing diameter variation of the discs, almost the same variations were observed between T_25 and T_50 discs. However, Figure 2 explains clearly that higher material removal had been observed with the T_50 disc. Wear rate is calculated using Archard's wear model (equation (4)); which gives valuable information about the wear mechanism of the discs. According to Figure 3, wear rate follows the standard wear diagram found in the literature (R Lewis, Dwyer-Joyce et al., 2010; R Lewis & Olofsson, 2004);

initially showing higher wear rate during the disc running-in stage, which happens shortly after the sliding contact between fresh and unworn metal surfaces is established. In this phase, modification of friction coefficient and wear rate are commonly observed (Blau, 2006).

Subsequently, steady-state wear can be observed for a couple of MGTs, followed by rapid and catastrophic wear. A slight reduction in wear rate for T_25 and T_50 is observed after 2.3 MGT due to contact pressure drop associated with contact patch elongation (Figure 4).

Maximum contact pressure of the T_25 rail disc rapidly declines and stabilises below 0.9 GPa. Wear rate reduces, but continuous plastic deformations occur as the contact pressure is still greater than the yield strength of the material. In the steady wear phase, contact pressures of T_flat and T_100 are nearly constant values. T_flat contact pressure is 460 MPa or 40% less than the yield strength of the material. Nonetheless, plastic deformation on the surface and wear have taken place, demonstrating that the rail wheel operated under the elastic zone can still undergo considerable plastic deformation. In 2002, Kapoor et al, (Kapoor, Franklin et al., 2002) published a paper that explains this phenomenon thoroughly. Rail surfaces are rough at the micro scale, and high shear stresses may occur only a few microns below the surface due to asperity contact. These asperities eventually lead to subsurface crack initiation leading to wearing off of the surface peaks. The wear of the disc is thus affected by the micro sliding on the surface. A detailed study of the wear mechanism is conducted using micro-roughness and microscopic images of the rail disc surface.

B. Rail Discs Surface Wear Analysis

1) Surface Roughness Data

At the end of the tests, surface roughness of each disc was measured using a Surtronic 3+ profilometer with 5 μm stylus tip, 0.8 mm cut-off length and 7.5 mm measured length. Surface profiles were obtained as shown in Figure 5, and roughness data of the discs are recorded in Table 3. According to Figure 5, waviness profiles of the rail discs appear as bumpy but blunt surfaces. But it is noticed that surface valleys at the Figure 5: b) and c) have sudden steep slopes. In addition, they are rougher than other surfaces due to severe sliding of trapped particles and/or material removal due to fatigue. Both flat and curved disc surfaces seem to stabilise in their wear mechanism. It is difficult to explain surface topology quantitatively with surface roughness parameters (R_a and R_q) but a combination of other parameters like skewness, kurtosis and bearing ratio etc, can be used to analyse surface topology quantitatively.

The roughness of the discs will decrease during the test and progressively descend to lower values, as other references have concluded (Nélias, Champiot et al., 1999; Wang, Wong et al., 2000; Zhang, Liu et al., 2013). According to Figure 5, roughness is relatively low for all discs except the T_100 disc, which demonstrates that the wear mechanism is still unstable, with high peaks value (R_p) (maximum height above the mean line within the sampling length) and greater average roughness (R_a) evident. R_{sk} is the skewness parameter of the surface, which represents asymmetry of the height distribution over the sampling length. This parameter is important as it provides information on the morphology of the surface texture. Positive values correspond to sharp high peaks distributed on a standard surface while negative values are found on surfaces with pores and scratches. The values were negative for three discs but positive for the T_100 disc, signifying that this disc has more scars, pores and other discrete types of damage on the surface. The kurtosis parameter R_{ku} presents information about spikiness of the height distribution over the surface. All discs have relatively blunt surface profiles (< 3) with the exception of T_flat (>3) which exhibits a more spiked surface. The bearing area parameter R_{mr} (%) gives more information about wear resistance of the worn surface. When R_{mr} is a higher percentage value for a specific depth below the surface (5% of the sample length amplitude), it means that a larger potential contact surface area exists. The greater values also suggest that lower contact pressures exist over the rail disc surface, therefore providing greater resistance to wear. In contrast, the T_100 rail disc has lower R_{mr} value (0.542%), which makes it more vulnerable to being worn due to lower true area of contact. According to the surface waviness profiles, the

curved surfaces are subjected to more wear damage as their profile has uneven surface irregularities when compared to the flat disc.

2)Macroscopic Wear of Rail Discs

Various images were taken of the surfaces after the tests were completed. The images provide additional information about the surface damage and changes in rail disc diameter. Figure 7 shows the damage that has been done on the surface due to high contact loading. The golden reddish colour and silver indicates that different levels of oxidation films were generated during the process. This disc was subjected to 2.5 million contact cycles, and oxidised layers were formed due to the thermal effect during dry contact. Different thickness of the oxidation layer can be a result of the different sliding levels in the contact interface, leading to different thermal profiles. Furthermore, it could be result of delamination of the oxidised film. Figure 7: b) clearly shows the elongation of the contact patch during the test. Due to contact area elongation, the contact patch becomes more like a line contact and reduces the maximum Hertzian contact pressure considerably. The wear rate, however, is not significantly mitigated as the contact pressure drops because, during the high contact loading conditions, subsurface damage occurs due to high shear stresses. When the contact load falls, previously-initiated subsurface cracks continue to propagate towards the surface until the material spalls off from the metal surface. After that, the wear rate is reduced accordingly due to the reduction of shear stress on the surface. Deters and Proksch (Deters & Proksch, 2005) demonstrated that the oxidised layer is worn off as large stamp-like flakes that could cause deep valleys in the contact zone.

The T_50 disc has more damage scars explaining the severity of the surface damage. Elongation of the contact zone is also evident from the damage observed on disc T_50. Due to this damage, the surface of the disc becomes wavier and with a high-amplitude profile as evidently shown Figure 5: c). The wear process should be more controlled because of the fact that contact pressure drops as the contact patch elongates. Instead, the wear rate increased after 1.8 MGT even though contact pressure reduced. This is because subsurface initiated cracks during the high contact loading propagated towards the surface due to the drop in contact pressure. Eventually, disc material is worn off as large delaminated particles. Figure 6: a) is a classic example of rolling contact fatigue failure of the rail material. From the particle size it is evident that subsurface initiated cracks had propagated along the surface as the T_50 curvature is more broadly distributed over the disc surface when compared to the T_25 disc. However, adhesive wear of the material can be observed in Figure 6: b) and d). The comparison of roughness profiles and Figure 6: b) reveal that the peak areas result in more sliding and RCF damage, while the valley areas are subjected to more adhesive wear as the worn particles squash through this region. Furthermore, Figure 6: d) also shows that more oxidation is evident in the sliding region. Figure 8 shows that a complex wear mechanism has taken place in the contact zone as adhesion, RCF wear and some ploughing are all observed. Bumpy peaks on the surface were generated, which can also be found in the roughness data and Figure 8: a) and b). The initial point of contact had higher contact pressure, resulting in the generation of subsurface cracks in that region. As the number of cycle progresses, the cracks develop toward the surface and spall off from the metal surface, causing high material removal rates near the center-line of the rail disc. This phenomenon is common for the other curved discs as well. Comparing roughness and wear data of disc T_100, it is evident that the rail disc is still wearing off the initial damage and the steady state wear mechanism has not yet stabilised. The sliding lines were subjected to oxidation, but surface damage is less severe than both T_25 and T_50 discs under the tested MGT levels.

The flat rail disc shows full contact of the disc surface as it has very few abrasive scars and predominantly adhesion wear marks on the surface as shown in Figure 9: b). Less wear is evident under 1.8 MGT traffic and due to the relatively low line-contact pressure.

3) Microscopic Wear of the Rail Disc

The literature (Deters & Proksch, 2005; Hardwick et al., 2014; Kapoor, Fletcher et al., 2005; Markov, 1995; Tyfour et al., 1995) has only explained the contact behaviour of the flat surface disc. It is difficult find a good study on the effect of the profiled discs on rail wheel contact under this level of MGTs. Consequently, in this work, surface replication was performed to study the material surface damage that occurred in the profiled T_50 rail disc. Scanning electron and light microscope images illustrate what damage exists on the material surface. Two types of wear zones are apparent at the tip of the curved wheel.

The tip of the curve wears off mainly due to rolling contact fatigue. Uneven material removal arising from variations of contact pressure and creep in the different wear zones may be observed (Figure 10: a)). Sliding areas appeared more compact and subjected to oxidation wear when compared to the adhesive wear zone.

Figure 10: b) shows the thin metal tongue structure that developed in the adhesive wear zone. This kind of tongue formation has been highlighted in the research on pearlitic rail steel by Deters and Proksch (Deters & Proksch, 2005). These metal tongues were generated due to higher plastic deformation in the sliding region. The higher stresses on the metal surface lead to the generation of laminar wear particles due to rolling contact fatigue. Close observation of the zone boundary in Figure 11 has shown that some cracks were initiated in the sliding area and develop into the adhesive wear zone. These cracks are probably a sign of the failing adhesive zone and expanding sliding zone through subsurface crack propagation toward the surface. The developed cracks spall the material and cause grooving in the boundary as shown in the corresponding surface waviness profile (Figure 5: c)).

Microscopic images of the replica using scanning electron microscopy (SEM) in the adhesive wear zone have identified surface damage that is the same shape as the particles formed during the tests (Figure 12 a) and Figure 13: a)). Also, it is observed that some metal tongue formation occurs in the sliding region that is likely due to flow of plastically deformed metal layer.

The collected particles are shown in Figure 13: a), obtained using TM3000 table top SEM. The measured particles were more like laminar flakes in a wide range of sizes. By looking at the size, shape and elemental composition, it may be observed that they are delaminated fatigue particles consisting of oxide and metal. Also, they have the same shape as the damage consistent with the adhesive wear regime. According to the literature, large flake-like particles arise due to the rolling contact fatigue wear mechanism resulting from the delamination process. Energy Dispersive Spectrometer (EDS) analysis of the particles (Figure 13: b)) show considerable amounts of iron and oxygen confirming a worn off oxidised layer.

Results of the rail discs highlight that different wear mechanisms exist on the rail wheel contact interface such as rolling contact fatigue, sliding and oxidation. Abrasive wear rarely exists as the both rolling discs have the same hardness. All this information emphasises the importance of contact profile on the wear mechanisms that exist in the rail-wheel contact.

4. Conclusion

Understanding of the wear mechanisms of the rail-wheel contact under different profile conditions is critical. In the practical scenario, the rail-wheel contact is neither a pure line contact nor a point contact. Different contact profiles exist as wear progresses and the effects of the contact conditions on the wear mechanisms are summarised as follows:

- Wear rate was plotted using Archard's law taking into consideration the different surface curvatures. It has been observed that different wear mechanisms exist and that wear rate is modified corresponding to the surface profile of the rail disc. Adhesive and RCF wear mechanisms dominated in this case study where externally applied traction was absent.

- The curved disc surfaces did not show significant wear in the running-in phase because damage occurred in the subsurface due to the high shear stresses there. Sudden spalling of material was eventually witnessed even under the low contact pressure in later contact cycles.
- The rail disc surface became relatively smooth once the steady-state wear mechanism is established. The variation of roughness parameters, including skewness and kurtosis, holds important information about the wear mechanisms.
- Different wear profiles exist due to variable surface waviness arising from delamination of the surface layer in the longitudinal direction. Intermittent measurement of surface parameters during the tests will provide more understanding about the wear transitions.
- All the rail disc surfaces were oxidised due to relatively high surface temperature at a micro-level asperity contact. These oxide layers are more prone to RCF failure by generating flake-like particles due to reduced fracture toughness of the iron oxide layer compared to the metal surface.
- Surface waviness and roughness should be included in the wear mode simulation of rail-wheel contact using appropriate material models to predict ratcheting behaviour of rail materials.

The above methodology will be further developed to understand wear behaviour of the curved discs and to improve modelling using appropriate material models.

Acknowledgements

This investigation has been performed with the assistance of the Banyo Pilot Plant Precinct and the Institute for Future Environments (IFE) at Queensland University of Technology. The authors would like to thank the staff of the IFE for all their technical support.

REFERENCES

Australian Standard : Railway Track Materials. Part 1: Steel Rails. AS1085.1-2002. (2002).

Bhushan, Bharat. (2013). Introduction to Tribology: Wiley. com.

Blau, Peter J. (2006). On the nature of running-in. Tribology International, 38(11), 1007-1012.

Bolton, PJ, & Clayton, P. (1984). Rolling—sliding wear damage in rail and tyre steels. Wear, 93(2), 145-165.

Chaboche, JL. (2008). A review of some plasticity and viscoplasticity constitutive theories. International Journal of Plasticity, 24(10), 1642-1693.

Dafalias, Yannis F., Kourousis, Kyriakos I., & Saridis, George J. (2008). Multiplicative AF kinematic hardening in plasticity. International Journal of Solids and Structures, 45(10), 2861-2880. doi: 10.1016/j.ijsolstr.2008.01.001

Deters, Ludger, & Proksch, Matthias. (2005). Friction and wear testing of rail and wheel material. Wear, 258(7), 981-991.

Epp, KJ, & Mutton, PJ. (2002). Wheel/Rail Interaction: Current'State of the Art'in the Australasian Railway Industry. CORE 2002: Cost Efficient Railways through Engineering, 9.

Evans, G. (2013). Managing rail profile. Ironmaking and Steelmaking, 40(2), 115-119. doi: 10.1179/1743281212Y.0000000033

Feigenbaum, Heidi P., Dugdale, Joel, Dafalias, Yannis F., Kourousis, Kyriakos I., & Plesek, Jiri. (2012). Multiaxial ratcheting with advanced kinematic and directional distortional hardening rules. International Journal of Solids and Structures, 49(22), 3063-3076. doi: 10.1016/j.ijsolstr.2012.06.006

Fries, Robert H, & Dávila, Carlos G. (1986). Analytical methods for wheel and rail wear prediction. Vehicle System Dynamics, 15(sup1), 112-125.

Green, M. R., Rainforth, W. M., Frolish, M. F., & Beynon, J. H. (2007). The effect of microstructure and composition on the rolling contact fatigue behaviour of cast bainitic steels. Wear, 263, 756-765. doi: 10.1016/j.wear.2007.01.070

Hardwick, C, Lewis, R, & Eadie, DT. (2014). Wheel and rail wear—Understanding the effects of water and grease. Wear, 314(1), 198-204.

Jamison, W. E. (1982). Wear of Steel in Combined Rolling and Sliding. A S L E Transactions, 25(1), 71-78. doi: 10.1080/05698198208983067

Kapoor, A., Fletcher, D. I., Franklin, F. J., Vasic, G., & Smith, L. (2005). Rail-wheel contact research at the University of Newcastle. Paper presented at the 11th International Conference on Fracture 2005, ICF11, March 20, 2005 - March 25, 2005, Turin, Italy.

Kapoor, A., Franklin, F. J., Wong, S. K., & Ishida, M. (2002). Surface roughness and plastic flow in rail wheel contact. Wear, 253(1-2), 257-264. doi: 10.1016/S0043-1648(02)00111-4

Kourousis, Kyriakos I., & Dafalias, Yannis F. (2013). Constitutive modeling of Aluminum Alloy 7050 cyclic mean stress relaxation and ratcheting. Mechanics Research Communications, 53, 53-56. doi: 10.1016/j.mechrescom.2013.08.001

Krishna, Shree, Hassan, Tasnim, Ben Naceur, Ilyes, Saï, Kacem, & Cailletaud, Georges. (2009). Macro versus micro-scale constitutive models in simulating proportional and nonproportional cyclic and ratcheting responses of stainless steel 304. International Journal of Plasticity, 25(10), 1910-1949. doi: http://dx.doi.org/10.1016/j.ijplas.2008.12.009

Lewis, R, Dwyer-Joyce, RS, Olofsson, Ulf, Pombo, J, Ambrósio, J, Pereira, M, . . . Kuka, N. (2010). Mapping railway wheel material wear mechanisms and transitions. Proceedings of the Institution of Mechanical Engineers, Part F: Journal of Rail and Rapid Transit, 224(3), 125-137.

Lewis, R, & Olofsson, Ulf. (2004). Mapping rail wear regimes and transitions. Wear, 257(7), 721-729.

Lewis, R., & Dwyer-Joyce, R. S. (2004). Wear mechanisms and transitions in railway wheel steels. Proceedings of the Institution of Mechanical Engineers, Part J: Journal of Engineering Tribology, 218(6), 467-478. doi: 10.1243/1350650042794815

Lewis, Roger, & Olofsson, Ulf. (2009). Wheel-rail interface handbook: CRC Press.

Marich, S., & Mutton, P.J. (1989). Materials developments in the australian railway industry-past, present and future. Paper presented at the The Fourth I.iternationa1 Heavy Haul Railway Conference, Brisbane, .

Markov, D. (1995). Laboratory tests for wear of rail and wheel steels. Wear, 181, 678-686.

Nélias, DMLFADR, Champiot, F, Girodin, D, Fougéres, R, Flamand, L, Vincent, A, & Dumont, ML. (1999). Role of inclusions, surface roughness and operating conditions on rolling contact fatigue. Journal of tribology, 121(2), 240-251.

Ozsarac, Ugur, & Aslanlar, Salim. (2008). Wear behaviour investigation of wheel/rail interface in water lubrication and dry friction. Industrial Lubrication and Tribology, 60(2), 101-107.

Pal, Sarvesh, Daniel, William J. T., Valente, Carlos H. G., Wilson, Andrew, & Atrens, Andrej. (2012). Surface damage on new AS60 rail caused by wheel slip. Engineering Failure Analysis, 22, 152-165. doi: 10.1016/j.engfailanal.2012.01.002

Ringsberg, J. W., Loo-Morrey, M., Josefson, B. L., Kapoor, A., & Beynon, J. H. (2000). Prediction of fatigue crack initiation for rolling contact fatigue. International Journal of Fatigue, 22(3), 205-215. doi: 10.1016/S0142-1123(99)00125-5

Saulot, A., Descartes, S., & Berthier, Y. (2009). Sharp curved track corrugation: From corrugation observed on-site, to corrugation reproduced on simulators. Tribology International, 42(11-12), 1691-1705. doi: 10.1016/j.triboint.2009.04.042

Sheng, Li, & Kahraman, A. (2011). A fatigue model for contacts under mixed elastohydrodynamic lubrication condition. International Journal of Fatigue, 33(3), 427-436. doi: 10.1016/j.ijfatigue.2010.09.021

Suda, Yoshihiro, Komine, Hisanao, Iwasa, Takashi, & Terumichi, Yoshiaki. (2002). Experimental study on mechanism of rail corrugation using corrugation simulator. Wear, 253(1–2), 162-171. doi: 10.1016/s0043-1648(02)00095-9

Takikawa, M., & Iriya, Y. (2008). Laboratory simulations with twin-disc machine on head check. Wear, 265(9-10), 1300-1308.

Timoshenko, S, & Goodier, JN. Theory of elasticity, 1951. New York, 412.

Tyfour, WR, Beynon, JH, & Kapoor, A. (1995). The steady state wear behaviour of pearlitic rail steel under dry rolling-sliding contact conditions. Wear, 180(1), 79-89.

Vasic, Gordana, Franklin, Francis J., & Fletcher, David I. (2011). Influence of partial slip and direction of traction on wear rate in wheel-rail contact. Wear, 270(3-4), 163-171. doi: 10.1016/j.wear.2010.10.012

Wang, W, Wong, PL, & Zhang, Z. (2000). Experimental study of the real time change in surface roughness during running-in for PEHL contacts. Wear, 244(1), 140-146.

Wilson, L. J., Hargreaves, D. J., Clegg, R. E., & Powell, J. (2006). Modifications of a rail/wheel wear simulator to measure rail curve lubricant performance. Paper presented at the 06 - International Tribology Conference, Brisbane, Australia. http://eprints.qut.edu.au/10903/

Zhang, Geng-pei, Liu, Xiao-jun, & Lu, Wen-long. (2013). Comprehensive evaluation of surface topography in running-in wear process. Paper presented at the Sixth International Symposium on Precision Mechanical Measurements.

TABLE I: CHEMICAL COMPOSITION OF MATERIAL

Chemical Element	Normal Rail Size (60kg)	Analysed Report From Redbank Foundry (average %)
Carbon %	0.65 -0.82	0.698
Manganese %	0.70 - 1.25	0.796
Silicon %	0.15 -0.58	0.451
Phosphorus %	0.025 max.	0.021
Sulphur %	0.025 max.	0.013
Aluminium %	0.005 max.	0.035
Nitrogen %	0.010 max.	-
Chromium (Cr)	0.15	0.099
Molybdenum (Mo)	0.02	0.017
Nickel (Ni)	0.1	0.023
Copper (Cu)	0.15	0.016
Tin (Sn)	0.04	-
Titanium (Ti)	0.025	0.002
Niobium (Nb)	0.01	0.01
Vanadium (V)	0.03	0.004
Lead (Pb)	-	<0.002
Boron (B)	-	0.002
Cu + 10Sn	0.45	-
Cr+Mo+Ni+Cu+V	0.3	0.136

TABLE II: FINAL CONDITION OF THE RAIL DISC

Disc sample no. and surface curvature	Final wear volume (mm^3)	Contact patch elongation (mm)	Final Hertzian contact pressure (GPa)	Initial Hertzian contact pressure (GPa)
Test 1 - 100mm	226.03	8.32	0.85	1.25
Test 2 - Flat	212.60	20	0.46	0.46
Test 3 - 50mm	1580.20	12.60	0.80	1.52
Test 4 - 25mm	1129.68	8.93	0.96	1.95

TABLE III :SURFACE ROUGHNESS PARAMETERS

Parameter	T_25	T_50	T_100	T_Flat
R_p (μm)	0.869	1.67	5.863	1.787
R_t (μm)	3.23	7.44	19.89	5.77
R_a (μm)	0.465	0.853	2.427	0.634
R_q (μm)	0.533	1.059	2.941	0.806
R_{sk}	-0.284	-0.068	0.154	-0.645
R_{ku}	2.540	2.729	2.611	3.458
R_{mr} %	8.426	3.688	0.542	1.875

Figures:

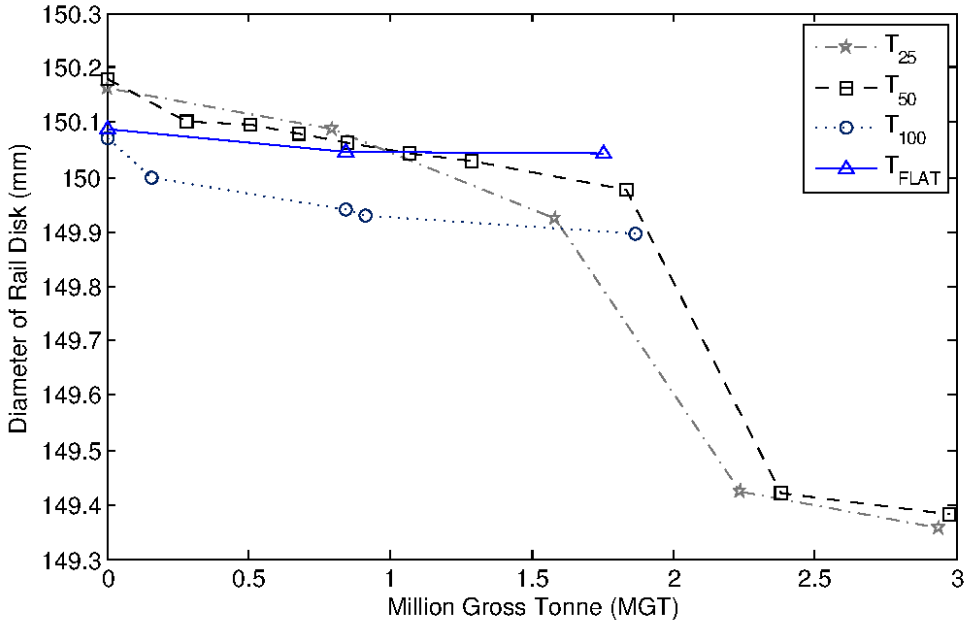

Figure 1: Wear rates in terms of diameter change

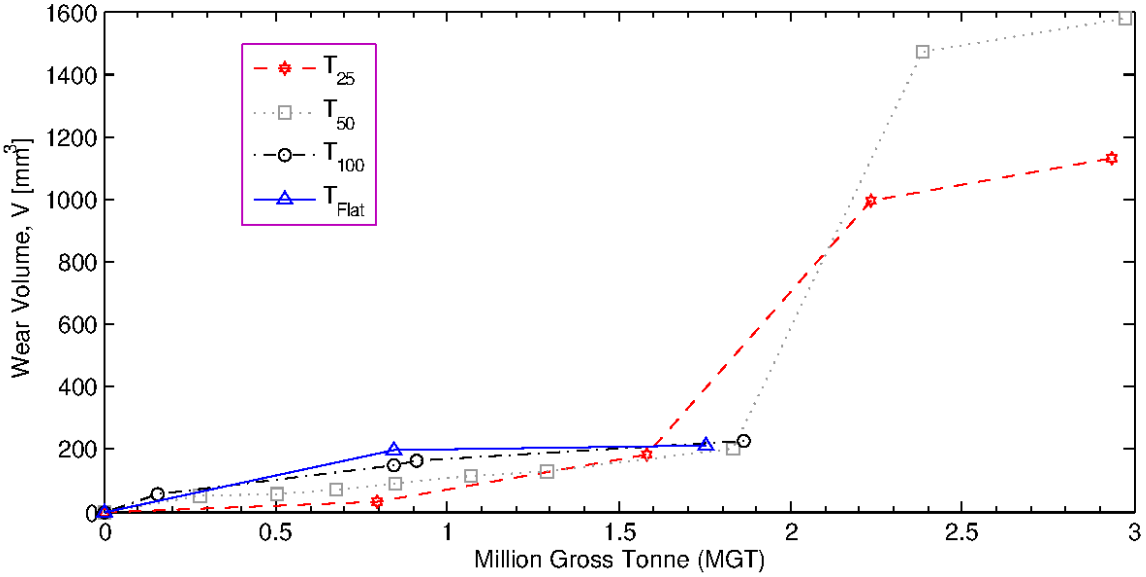

Figure 2: Wear volume of rail discs

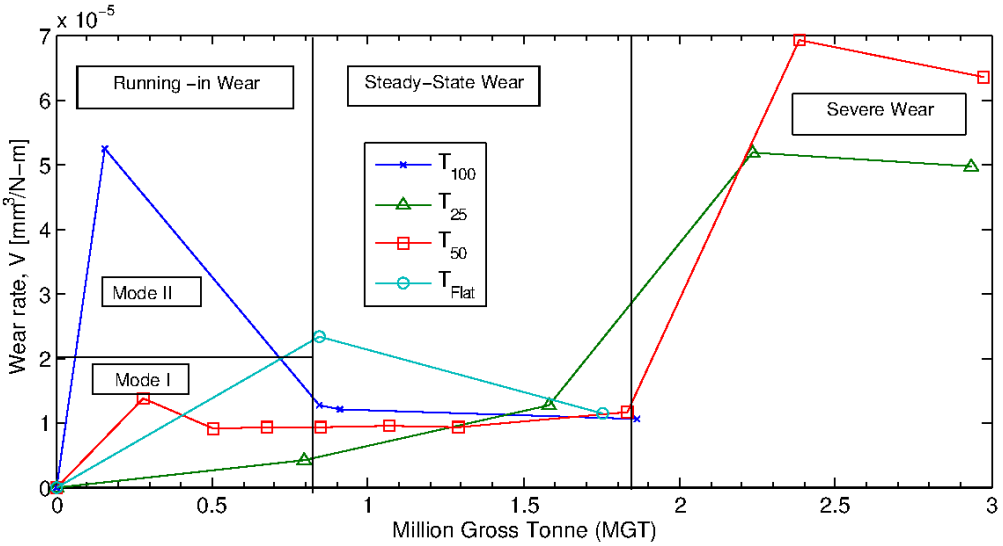

Figure 3: Wear rate of rail disc

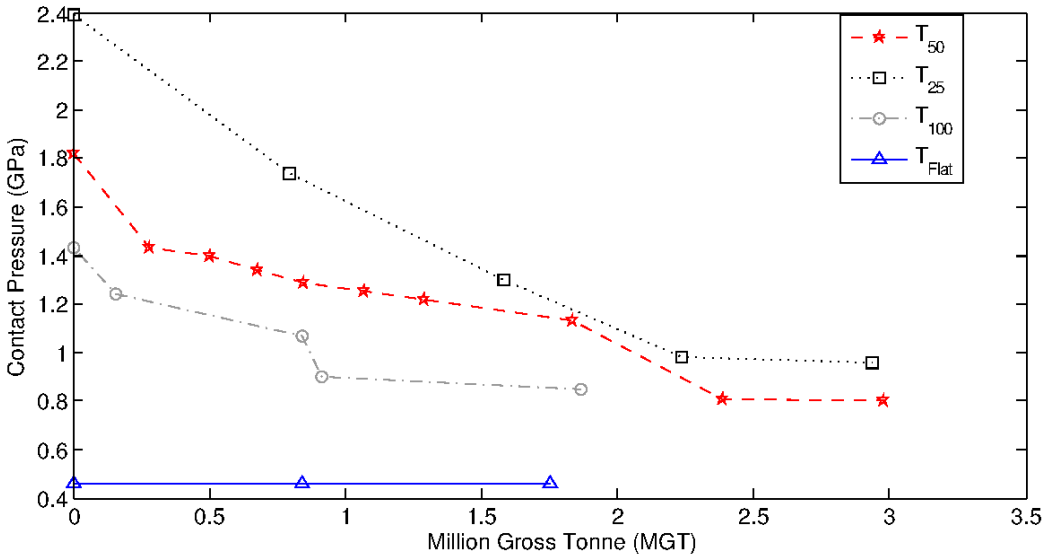

Figure 4: Contact pressure variation during the test

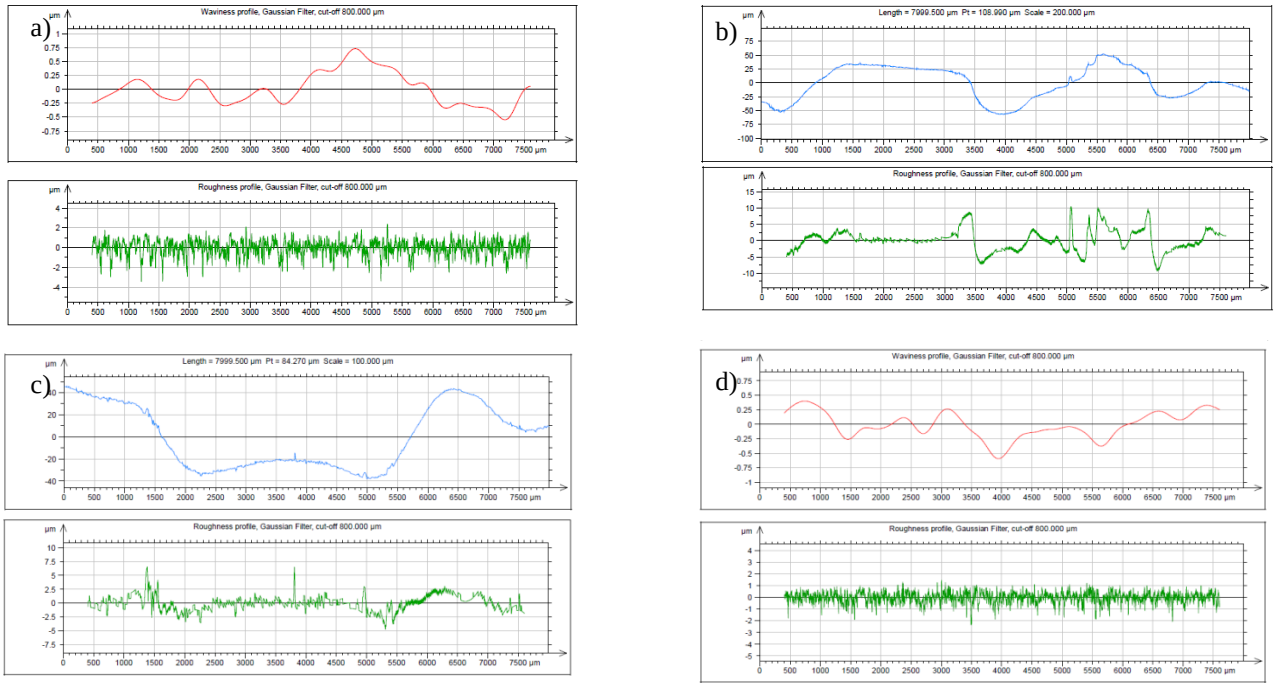

Figure 5: Rail surface roughness measurements of rail discs: a) T_ flat, b) T_100, c) T_50 and T_25

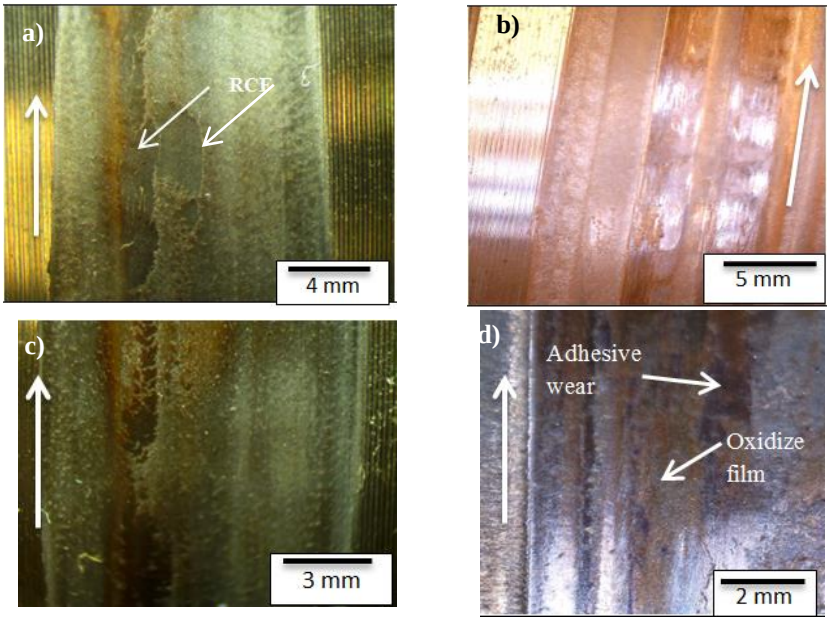

Figure 6: Surface wear of the rail disc T_50: a) RCF wear, b) sliding and adhesive wear zones, c) adhesive wear and d) oxidised film

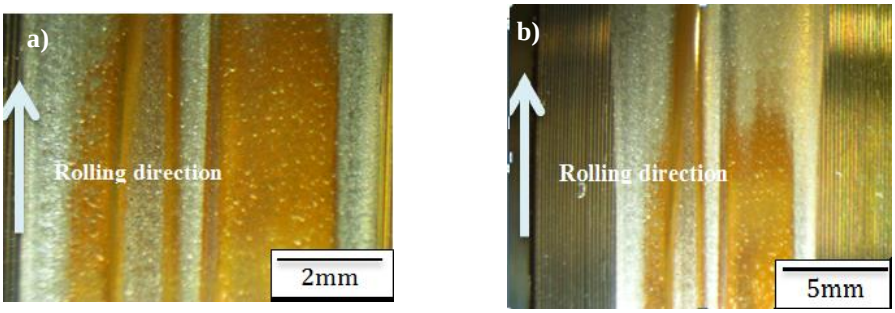

Figure 7: Surface wear of T_25, a) different oxidation Level and b) Contact patch elongation

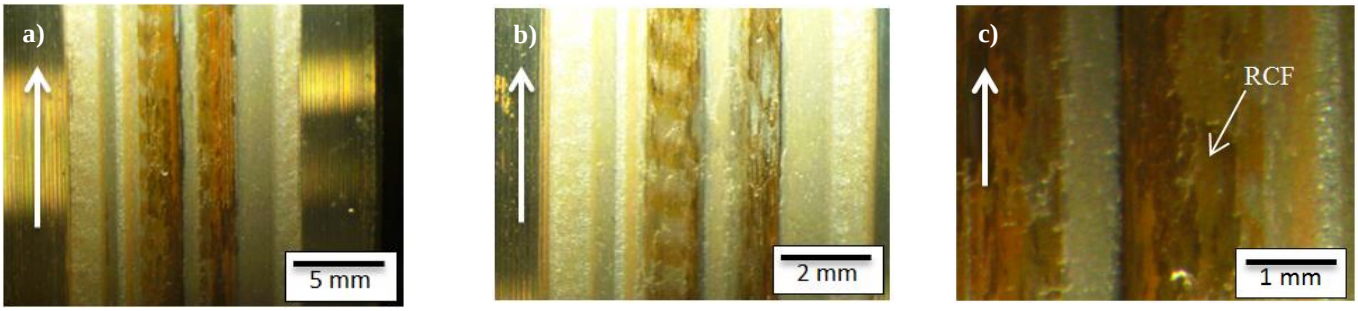

Figure 8: Surface wear of rail disc T_100; a) Sliding and adhesive wear, b) Distinct oxidation level and c) RCF wear

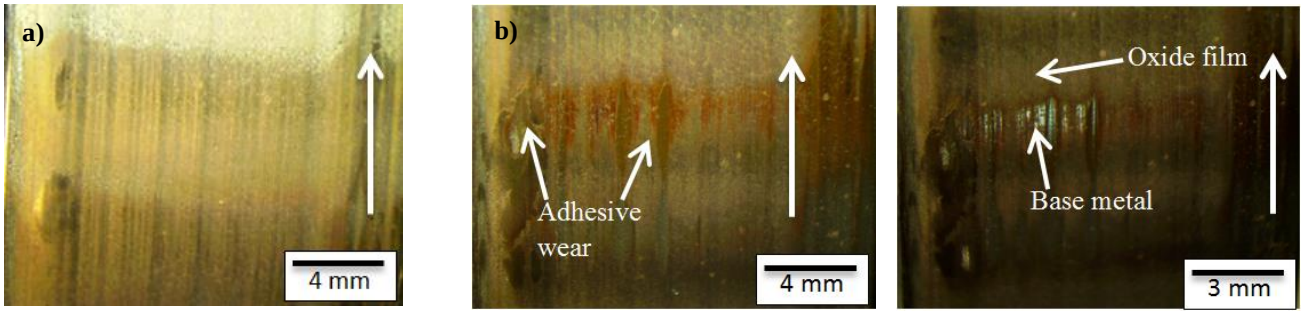

c)

Figure 9: Surface wear of rail disc T_flat; a) High wear in edges, b) Adhesive wear, and c) Wear of oxidised film

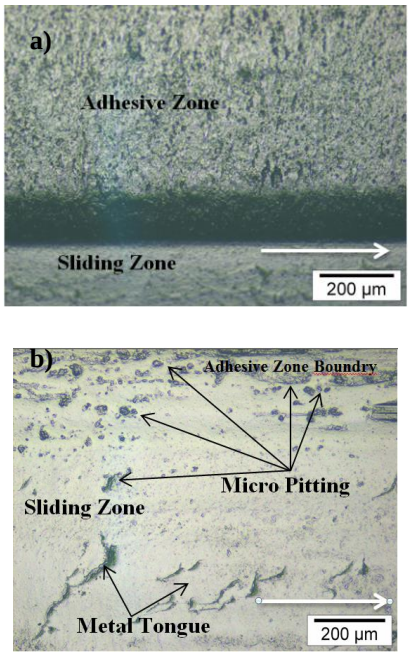

Figure 10: Wear zone of rail disc T_50; a) Different level of wear zone and b) Prominent surface damage

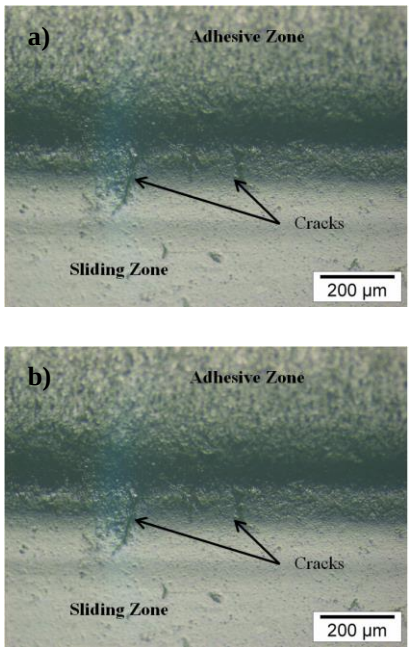

Figure 11: Crack development in wear zone boundary; a) Cracks development between two zones and b) Sliding region elongation

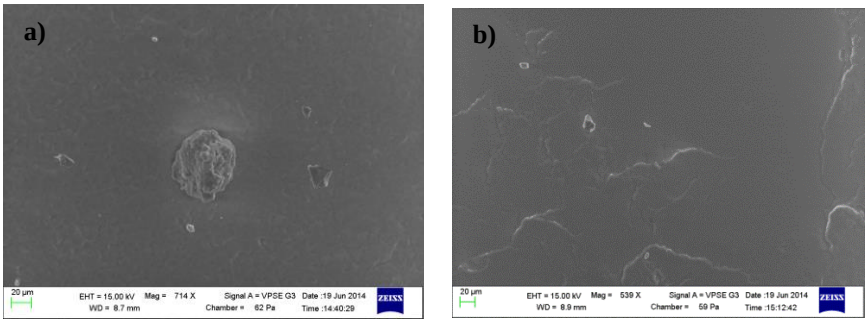

Figure 12: SEM images of surface replica; a) Surface damage in adhesive zone and b) Metal tongues in sliding zone

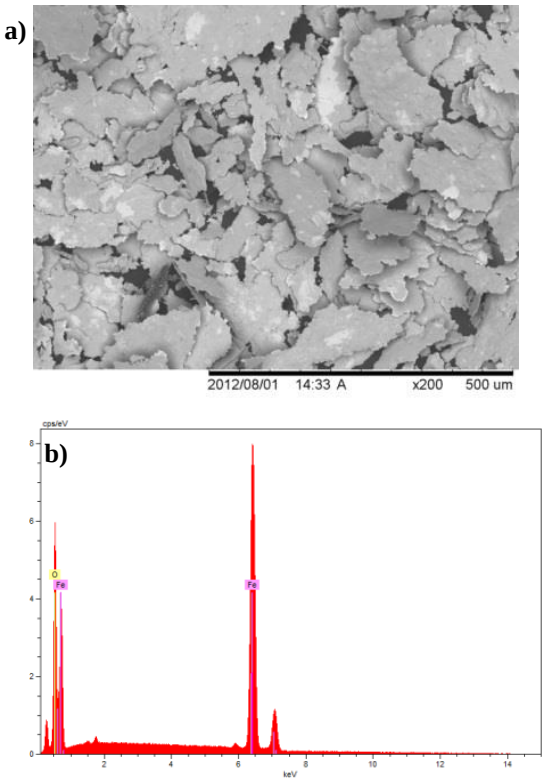

Figure 13: Particle generated during T_50 and EDS of particles